

Concentration-Dependent Dimerization of Staphylokinase Variants with Engineered Surface Charges

Michal Nemergut¹, Monika Štulajterová², Rostislav Škrabana³, Andrej Hovan^{1,2},
Ľuboš Ambro¹, Alan Strunga^{5,6}, Zbyněk Prokop^{5,6}, Jiří Damborský^{5,6},
Mária Tomková¹, Erik Sedlák^{1,4*}

¹Center for Interdisciplinary Biosciences, P. J. Šafárik University in Košice, Jesenná 5, 04154 Košice, Slovakia

²Department of Biophysics, Faculty of Science, P. J. Šafárik University in Košice, Jesenná 5, 04154 Košice, Slovakia

³Institute of Neuroimmunology, Slovak Academy of Sciences, Dúbravská cesta 9, 845 10 Bratislava 45, Slovakia

⁴Department of Biochemistry, Faculty of Science, P. J. Šafárik University in Košice, Moyzesova 11, 04154 Košice, Slovakia

⁵Loschmidt Laboratories, Department of Experimental Biology and RECETOX, Faculty of Science, Masaryk University, Kamenice 5/C13, 625 00 Brno, Czech Republic;

⁶International Clinical Research Center, St. Anne's University Hospital, Pekarska 53, 656 91 Brno, Czech Republic

* To whom correspondence should be addressed:

Center for Interdisciplinary Biosciences, P. J. Šafárik University in Košice, Jesenná 5, 04154 Košice, Slovakia; email: erik.sedlak@upjs.sk

Abstract

Staphylokinase (SAK) is a promising third-generation thrombolytic protein, but its clinical potential is limited by immunogenicity and stability concerns. The conformational and colloidal stabilities of four SAK variants – SAK 42D, SAK STAR, and their non-immunogenic derivatives SAK 42D 3A and SAK STAR 3A - were evaluated using differential scanning calorimetry (DSC), dynamic light scattering (DLS), and aggregation kinetics assays. DSC analyses revealed that thermal denaturation of all variants proceeds via two consecutive irreversible steps, with transition parameters strongly dependent on scan rate and protein concentration. SAK STAR variants exhibited markedly exothermic first transitions and reduced scan rate dependence, suggesting stabilization of intermediate states and suppression of aggregation. In contrast, SAK 42D variants exhibited endothermic or weakly exothermic first transitions and a higher aggregation propensity, correlating with reduced conformational stability and formation of less stable dimers. Colloidal stability tests showed that SAK STAR and SAK STAR 3A remained largely aggregation-resistant, whereas SAK 42D and SAK 42D 3A aggregated rapidly at elevated temperatures ($>51^{\circ}\text{C}$ and $>38^{\circ}\text{C}$, respectively), following apparent second-order kinetics. DLS confirmed concentration-dependent dimerization in all variants, with SAK 42D 3A displaying pronounced polydispersity and instability. We could rationalise this behaviour in the context of engineered surface charges. Our results demonstrate that SAK variant stability is shaped by a complex interplay between primary sequence, dimerization behaviour, and aggregation propensity, guiding the design of clinically viable thrombolytic agents and their formulations.

Introduction

Staphylokinase (SAK) is a 15.5 kDa protein secreted by certain strains of *Staphylococcus aureus* following lysogenic transformation by bacteriophages [Lack 1948]. SAK has recently attracted significant attention due to its efficiency to activate plasminogen in a ternary complex SAK-plasmin-plasminogen [Alasheev et al. 2023, Gusev et al. 2021, Nedaeinia et al. 2020, Nikitin et al. 2021]. The seemingly monomeric protein does not contain any posttranslational modifications and contains no disulfide bridge. SAK thus offers an advantage over other thrombolytic agents due to its simple protein scaffold. Moreover, SAK has high fibrin selectivity, meaning it converts plasminogen only near the thrombus and does not induce systemic plasminogen activation [Lijnen 1991], thereby reducing bleeding complications. There are several well-characterized natural variants of SAK, which differ at amino acid positions 34, 36, and 43: 42D - Gly34, Arg36, Arg43, STAR - Ser34, Gly36, His43 and Φ C - Gly34, Gly36, His43 (Figure 1 and Figure S2). Very recently, we have shown that although SAK 42D and STAR have similar conformational properties at physiological temperatures, their thermal stabilities assessed by circular dichroism in the far-UV region and intrinsic tryptophanyl fluorescence significantly differ [Štulajterová et al. 2025].

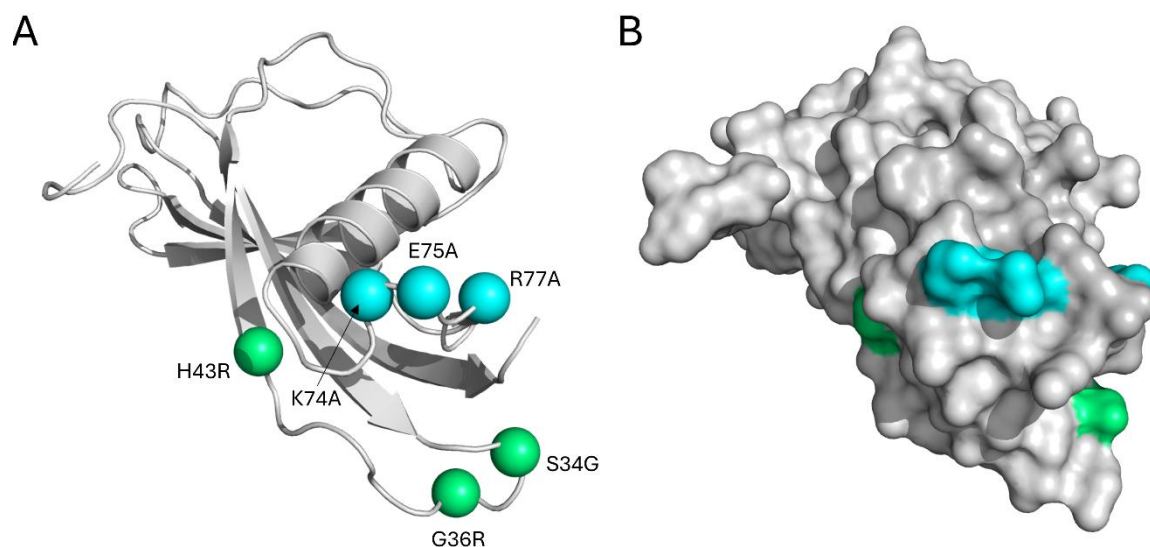


Figure 1. Visualization of the SAK STAR structure (PDB 2SAK) with depicted sites of amino acid variability. (A) Highlighted in green are substitutions in SAK 42D leading to lower stability in comparison with SAK STAR. The positions highlighted in blue correspond to alanine substitution sites in less immunogenic SAK versions designated as SAK 3A. (B) All six modified residues are exposed on the protein molecular surface.

SAK is immunogenic; its repeated administration leads to the production of neutralization antibodies and may potentially trigger an inflammatory reaction [Vanderschueren et al. 1994], which significantly limits its widespread clinical use. Significant effort was devoted to the development of SAK variants with reduced immunoreactivity. This goal was achieved by substituting three surface-exposed charged amino acids, Lys74, Glu75, and Arg77, with alanines (designated in our work as 3A variants; Figure 1) resulting in a 200-fold decrease of neutralizing antibody production [Collen et al. 1997].

The major physico-chemical properties, which define critical limitation of an application of (therapeutic) proteins, are their conformational and colloidal stabilities [Frokjaer & Otzen 2005]. Differential scanning calorimetry (DSC) is a powerful technique to characterize the energetics and mechanisms of temperature-induced conformational changes in proteins [Chen et al. 1999, Carrillo & Semple 2024]. One of the major advantages of DSC is its ability to distinguish transitions that are difficult to detect and to differentiate from other methods, such as spectroscopic approaches [Sedlak et al. 2015]. DSC can help reveal mechanisms related to conformational changes in proteins [Ramsay et al. 1989, 1990], thermodynamic analysis of oligomeric or multidomain proteins [Pina et al. 2003, Nemergut et al. 2023], or analysis of otherwise difficult to study strong protein-protein interactions [Brandts & Lin 1990, Nemergut et al. 2021].

In this study, we investigated four well-defined SAK variants with distinct genetic origins and prior characterization: (i) SAK 42D corresponds to a naturally occurring staphylokinase variant originally cloned and expressed from a lysogenic *Staphylococcus aureus* phage and biochemically characterized by Behnke and Gerlach [Behnke & Gerlach 1987]; (ii) SAK STAR is a distinct natural/recombinant variant isolated and characterized by Collen and colleagues, who demonstrated its thrombolytic activity and favorable pharmacological properties [Collen et al. 1992]; (iii) SAK STAR 3A was engineered from SAK STAR by substituting three surface-exposed charged residues (K74A, E75A, R77A) to reduce immunogenicity while preserving thrombolytic potency [Collen et al. 1997]; (iv) SAK 42D 3A was constructed in our laboratories by introducing the same 3A substitutions into the SAK 42D background to enable direct assessment of the effects of these mutations on conformational and colloidal stability [Štulajterová et al. 2025].

We have analyzed conformational and colloidal stabilities of these SAK variants by using DSC and dynamic light scattering (DLS). The purpose of these analyses was to determine and correctly describe the process of thermal denaturation of the studied SAK variants and determine the relationship, if any, between their conformational and colloidal stabilities. We

show that the SAK variants tend to dimerize in concentration- and temperature-dependent manners. Variants SAK 42D and SAK 42D 3A tend to precipitate due to significantly compromised conformational stabilities and likely due to the formation of less stable dimeric structures.

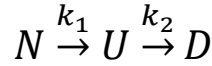
Material and methods

SAK Purification

For SAK purification, bacterial cell pellets were resuspended in lysis buffer (50 mM Hepes, 200 mM NaCl, 1 mM EDTA, 7 mM lysozyme, 10 μ M leupeptin, and 1 μ M pepstatin). Cells were lysed by sonication (Branson Sonifier 450, Thermo Fisher Scientific, USA), and lysates were centrifuged (30 min, 17 500 g, 4 °C). Supernatants were applied to a Ni-NTA gravity column (Thermo Fisher Scientific) equilibrated with 50 mM Hepes, 200 mM NaCl. After washing with the same buffer containing 40 mM imidazole, proteins were eluted with 250 mM imidazole and 10% glycerol. Eluates were concentrated using Amicon® Ultra (10 kDa MWCO, Merck, Germany) and further purified by size-exclusion chromatography (Superdex 75 Increase 10/300 GL, 50 mM phosphate buffer, pH 7.5). Purity was verified by 15% SDS-PAGE with InstantBlue Coomassie staining (Sigma-Aldrich, USA). Fractions of highest purity were pooled, flash-frozen, and stored at -80 °C. The results of SAK variant purification, including size-exclusion chromatograms and SDS-PAGE, are shown in [Figure S1](#).

Differential scanning calorimetry (DSC)

DSC experiments were carried out on a VP-Capillary DSC system (Microcal Inc., acquired by Malvern Instruments Ltd.). An extra pressure of 65 psi was maintained during all DSC runs to prevent possible degassing of the solutions on heating. Thermograms were corrected by subtraction of the so-called chemical baseline, i.e., the sigmoidal curve connecting the signal of excess heat capacity of the native and denatured states, and normalized to the molar concentration of the protein. Concentration dependence experiments have been performed at a scan rate of 1.5 °C/min at four concentrations: 0.5 mg/mL (32 μ M), 1.0 mg/mL (64 μ M), 1.5 mg/mL (96 μ M) and 2.0 mg/mL (128 μ M). Scan rate dependence experiments have been performed at protein concentration 1.0 mg/mL at four different scan rates: 0.5, 1.0, 1.5, and 2.0 °C/min. Analysis of the DSC scans has been performed according to the model of thermal denaturation consisting of two consecutive irreversible steps introduced by Lyubarev and Kurganov [[Lyubarev & Kurganov 1998](#)]:



The excess heat capacity, parameter measured in the DSC experiments, is expressed by the general equation satisfying the model:

$$C_p^{ex} = \frac{\Delta H_1 k_1}{v} \exp\left(-\frac{1}{v} \int k_1 dT\right) + \frac{\Delta H_2 k_2}{v} \exp\left(-\frac{1}{v} \int k_2 dT\right) \int \left[k_1 \exp\left(\frac{1}{v} \int (k_2 - k_1) dT\right) \right] dT$$

(Equation 1)

where ΔH_1 and ΔH_2 are calorimetric enthalpy changes for the first and second steps, respectively.

The rate constants, k_1 and k_2 , dependences are described by the Arrhenius equation, $k=A \exp(-E_a/RT)$, where A is the pre-exponential factor, E_a is the energy of activation, and R is the gas constant. Alternative form of the Arrhenius equation:

$$k \text{ (min}^{-1}\text{)} = \exp\left(\frac{E_a}{R} \left(\frac{1}{T^*} - \frac{1}{T}\right)\right)$$

(Equation 2)

in which A is replaced by the parameter T^* with clear physical meaning: T^* is the temperature at which rate constant equals 1 min^{-1} .

Colloidal stability

The colloidal stability of the studied SAK variants has been analysed by monitoring kinetics of aggregation by absorbance at 280 nm. We tested the colloidal stability of all variants at 1.0 mg/mL at four different temperatures related to the T_{trs} , apparent transition temperature obtained from DSC experiment, of the corresponding SAK variant: T_{trs} , $T_{trs} + 3^\circ\text{C}$, $T_{trs} + 6^\circ\text{C}$, and $T_{trs} + 9^\circ\text{C}$. The aggregation dependence was analyzed by a single exponential function:

$$A(t) = A_0 \exp(-kt) + A_{final}$$

(Equation 3)

where k is rate constant of aggregation, A_0 and A_{final} are absorbances at $t=0 \text{ min}$ and $t=\infty \text{ min}$, respectively.

Molecularity of reaction

The molecularity of reaction has been determined from the equation [Guthe et al. 2004]:

$$\log\left(\frac{1}{k}\right) = \text{const} - (n - 1)\log[M_0]$$

(Equation 4)

where k is the rate constant of aggregation obtained at $T_{trs} + 3^{\circ}\text{C}$ at three different concentrations of SAK variants: 0.5, 1.0, and 1.5 mg/mL. The parameter M_0 corresponds to the protein concentration at $t=0$ min, and n is the reaction order.

Light scattering

Dynamic light scattering (DLS) and static light scattering (SLS) were measured partly at constant temperature and partly in thermal denaturation experiments. When needed, SAK samples were concentrated by ultracentrifugation adopting 3 kDa molecular weight cut-off membranes. Before measurements, a stream of filtered argon was used to remove dust particles from the plasticware and 10-30 μL of the protein solution was centrifuged in 0.5 mL polypropylene microtubes at $21000 \times g$ at 25°C for 30-60 min to sediment aggregates and remaining dust particles. Constant temperature DLS was measured at three protein concentrations (STAR: 1.0, 2.2 and 5.0 mg/mL, STAR 3A: 1.0, 1.9 and 8.7 mg/mL, 42D: 1.0, 2.5 and 10.8 mg/mL, 42D 3A: 1.0, 1.2 and 3.7 mg/mL). In the text, these concentrations are referred as low, medium, and high, respectively. Four microliters of protein solution in a COC disposable cuvette (Wyatt Technology) were analysed at 25°C by a DynaPro NanoStar instrument with a red 658 nm laser and 90° scattering angle for both DLS and SLS. Data collection and processing were controlled by DYNAMICS software (version 7.10.0.21, Wyatt Technology). DLS autocorrelation functions were collected with a five second acquisition time, each measurement averaged 10 acquisitions, and 10 measurements were performed per sample. To cull the data deteriorated by dust or protein aggregates, an automatic filtering of autocorrelation functions was applied for baseline threshold and sum-of-squares error of cumulants fit. After filtering, at least 70 % of the original data remained for evaluation. Thermal denaturation experiments were conducted in COC cuvettes filled with 20 μL of 1 mg/mL protein. Temperature scan rate was $1.5^{\circ}\text{C}/\text{min}$ in the range 25 - 80°C . SLS and DLS data were acquired every 40 seconds, with 1 second acquisition time, and 10 acquisitions were averaged per time point. Thermal denaturation was repeated twice for each protein.

The apparent diffusion coefficient D_{app} and polydispersity were determined by cumulants analysis of autocorrelation function [Koppel 1972], as implemented in the Wyatt cumulant analysis method used by DYNAMICS. Hydrodynamic radius (R_h) was derived from D_{app} using Stokes–Einstein–Sutherland equation assuming spherical particles. The apparent fraction of (globular) dimers was estimated from measured R_h using theoretical R_h of monomer and dimer, as implemented by Apparent Fraction Calculator in DYNAMICS, assuming no higher oligomers present. Colloidal stability of SAK variants at 25°C was assessed from the

concentration-dependent changes in D_{app} . Multimodal autocorrelation curves of SAK STAR variant in the temperature region 60-66 °C were analysed by regularization analysis of autocorrelation functions to determine the distribution of particle sizes [Provencher 1979] by DYNAL regularization algorithm in DYNAMICS.

SLS intensity I_{SLS} was used to monitor changes in molecular weight of proteins during thermal scan in the temperature region preceding precipitation. Assuming Rayleigh scattering from SAK protein particles < 10 nm and a constant mass per volume protein concentration during thermal scan, the I_{SLS} is proportional to the mass-averaged molecular weight of particles [Wyatt 1993], therefore the protein oligomerization can be directly monitored. Temperature transition point of thermal denaturation and precipitation of proteins during thermal scan was detected by a sudden decrease of sample optical transmittance, deduced from the ratio of forward monitor and laser monitor readings.

Results

Analysis of temperature dependence of heat capacity of protein in thermal transition can provide detailed information about its nature such as reversibility and number of steps of the protein thermal transition. Figure 2 shows DSC scans of three representative transitions: (i) reversible two states, (ii) irreversible two states, and (iii) thermal transition of SAK. Reversible and irreversible transitions (upon chemical baseline subtraction) differ by a symmetry: a reversible transition is symmetrical and an irreversible one is asymmetrical with a steeper decrease in heat capacity on the hotter side [Sanchez-Ruiz et al. 1988, Sanchez-Ruiz 1992]. DSC scans of the studied SAK variants are also asymmetrical but with an unusually extended transition on the hotter side of the curves, in contrast with the one-step irreversible transition.

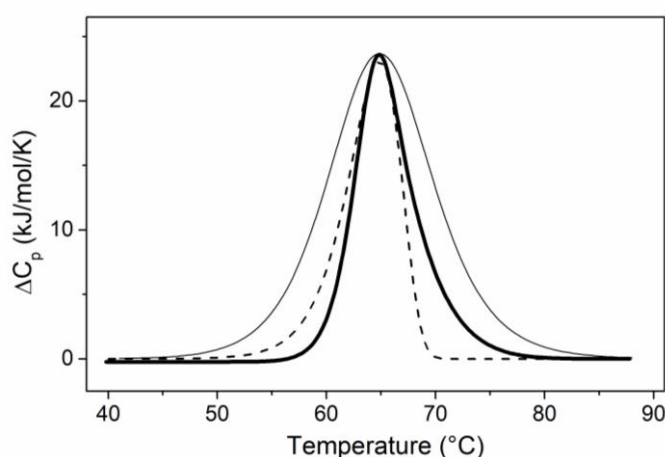


Figure 2. Illustrative comparison of the shape of DSC scans of reversible (thin line) and irreversible (dashed line) thermal transitions with the representative example of thermal transition of the studied SAK variants (thick line).

Analysis of SAK thermal transitions reveals that SAK thermal denaturation is irreversible and depends both on scan rate and protein concentration. The apparent melting temperature of SAK variants increases with heating scan rate and decreases with increasing protein concentration (Figure S3). Irreversibility and observed scan rate dependences of thermal transitions of SAK variants on scan rate of heating and protein concentration clearly indicate involvement of kinetically driven steps(s) in the process of thermal denaturation. Based on the observed dependences and the asymmetry of DSC scans, we assume that SAK thermal transitions consist of two consecutive irreversible steps as described by Lyubarev and Kurganov [Lyubarev & Kurganov 1998].

Differential scanning calorimetry analyses of SAK variants.

Scan rate dependences. Transitions of four variants of SAK: SAK 42D, SAK 42D 3A, SAK STAR, and SAK STAR 3A have been analyzed. For all variants, we performed two sets of measurements: (i) scan rate dependences of proteins at 1 mg/mL at scan rates 0.5, 1.0, 1.5, and 2.0 K/min and (ii) protein concentration dependences at 1.5 K/min for 0.5, 1.0, 1.5, and 2.0 mg/mL (Figures S4-S7). DSC thermal transitions of the studied proteins at 1.0 mg/mL and scan rate 1.5 K/min were, for comparison, plotted in Figure 3. Obtained heat capacities temperature dependences have been fitted by Equation (1), derived by Lyubarev and Kurganov [Lyubarev & Kurganov 1998]. All fits were in excellent agreement with experimental data on heat capacity. Obtained enthalpies of the two transitions of thermal denaturation are positive only for the SAK 42D. For all other SAK variants, the enthalpies of the first transition are negative

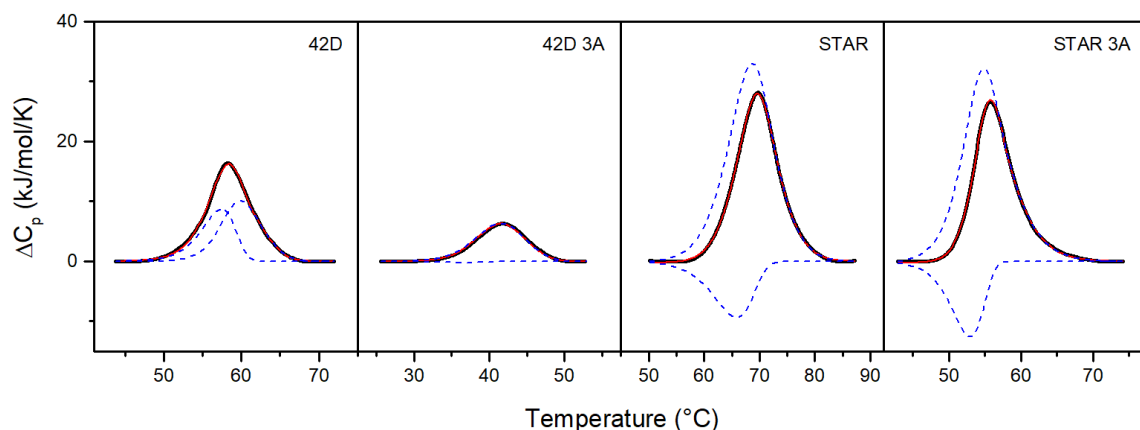


Figure 3. DSC thermal transitions of the studied SAK variants with corresponding fits according the model of Lyubarev and Kurganov (Equation 1). The experimental scans are shown as black solid lines, the individual thermal transitions obtained from the fit according the Equation 1 are shown as dashed blue lines, and the solid red lines show the sum of the dashed blue lines.

(Figure 3). Therefore, these unusual observations have been analyzed in more detail. All DSC measured transitions have been numerically fitted by Equation 1 and obtained parameters were summarized in Table S1 and plotted in the corresponding dependences shown in Figures 4. The plots showing the dependences of activation energy (E_{a1} , E_{a2}) and transition temperature (T_1^* , T_2^*) values on scan rate indicate that E_a is relatively independent on scan rate of heating with small tendency to approach the values of both transitions, due to slightly decreasing E_{a1} and small increasing tendency of E_{a2} . On the other hand, the entropic part of the free energy of activation, reflected by the values T^* , shows a clear difference between values of the first and the second steps due to significant decrease in the T_2^* values. This suggests an increase in the entropy of the free energy of activation. The values of calorimetric enthalpies obtained from the fits, corresponding to the energy absorbed and/or released, of both steps are relatively independent on the heating scan rate (Table S1). In these cases, the commonly used analysis of DSC scans involving the comparison of calorimetric and van't Hoff enthalpies is not applicable due to irreversible and kinetically driven nature of thermal transitions of studied SAK variants. The $\Delta H_{cal}/\Delta H_{vH}$ criterion is valid only for reversible equilibrium transitions; therefore, no conclusions regarding two-state behavior or intermediates can be drawn from this analysis [Sturtevant 1987].

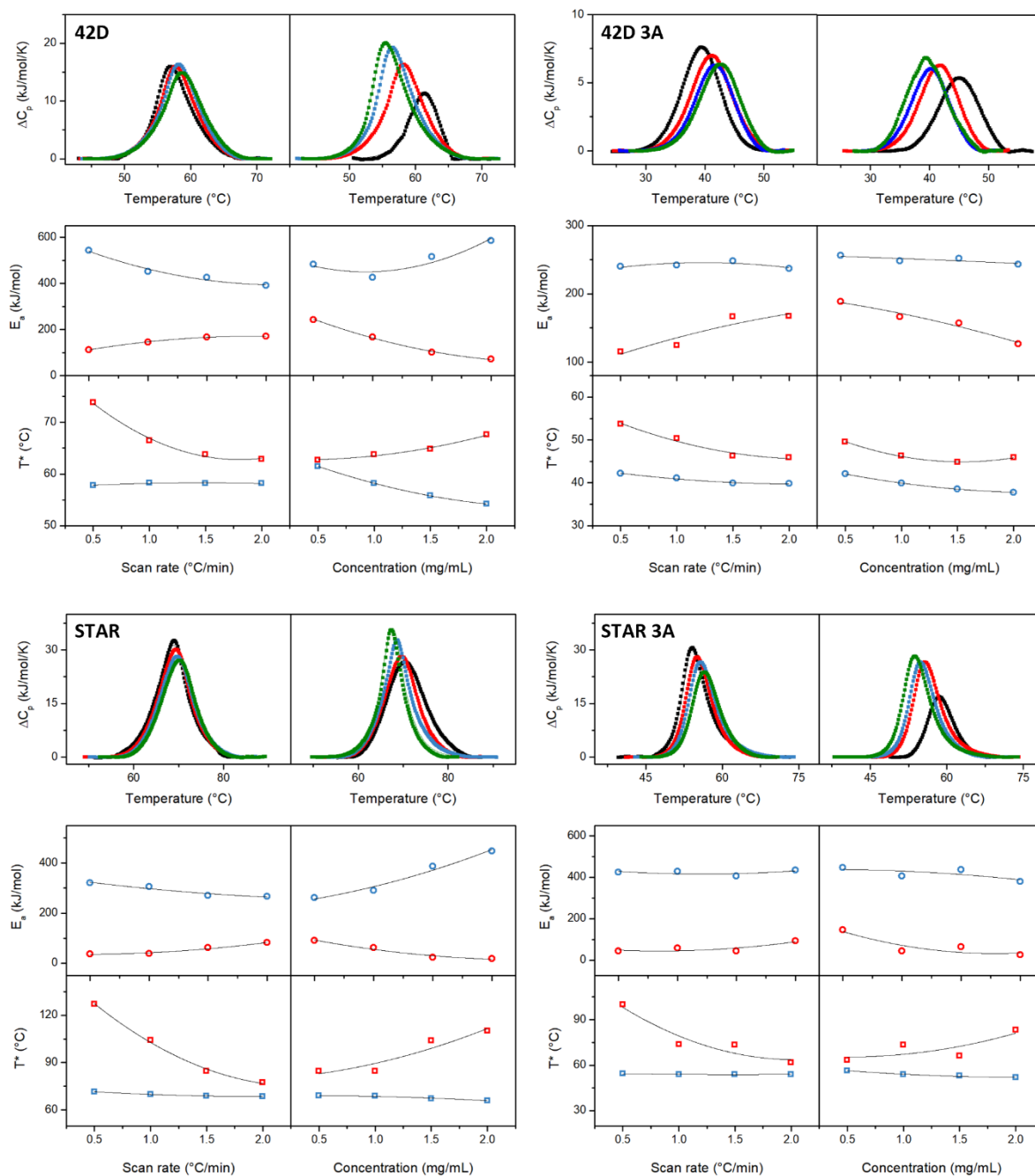


Figure 4. DSC thermograms of the studied SAK variants showing thermal transitions as a function of scan rate (left panels) and protein concentration (right panels). Measurements were performed at four scan rates - 0.5 °C/min (black), 1.0 °C/min (red), 1.5 °C/min (blue), and 2.0 °C/min (green) - and at four protein concentrations - 0.5, 1.0, 1.5, and 2.0 mg/mL, using similar color coding. During the scan rate dependence measurements, the protein concentration was 1 mg/mL, and during the concentration dependence measurements, the scan rate was 1.5 °C/min. Corresponding dependencies of the activation energy (E_a) and transition temperature (T^*) values were derived according to Equations (1) and (2). E_a and T^* values for the first transition step (E_{a1} and $T1^*$) are shown in blue, and those for the second transition step (E_{a2} and $T2^*$) in red. Trend lines are included for visual guidance only.

Protein concentration dependences. Analogous analysis of thermal transitions of SAK variants, measured by DSC, in dependence on protein concentration, reveals several apparent tendencies of the obtained parameters E_a and T^* :

(i) the shape of the heat capacity dependences on temperature changes in the case of SAK 42D and SAK STAR. The DSC transitions become steeper with increasing protein concentration. This narrowing is less apparent in the SAK 3A variants.

(ii) E_{a1} increases in SAK 42D and SAK STAR and is relatively independent in the SAK 3A variants on the protein concentration.

(iii) E_{a2} always decreases with protein concentration.

(iv) the difference of T^* values between the first and the second steps increases with protein concentration for all variants besides SAK 42D 3A. In this case, the difference between T_1^* and T_2^* values is relatively constant over the studied protein concentration.

Colloidal stabilities of SAK variants. Observed protein concentration dependences of SAK thermal denaturation as well as a presence of signs of aggregations in samples of SAK 42D and SAK 42D 3A led us to analysis of colloidal stabilities of all SAK variants. We tested the colloidal stability of all variants at 1.0 mg/mL at four different temperatures related to the T_{trs} of the corresponding SAK variant: T_{trs} , $T_{trs}+3^\circ\text{C}$, $T_{trs}+6^\circ\text{C}$, and $T_{trs}+9^\circ\text{C}$, i.e. $T_{trs} = 55^\circ\text{C}$ for SAK 42D, $T_{trs} = 39.4^\circ\text{C}$ for SAK 42D 3A, $T_{trs} = 67.7^\circ\text{C}$ for SAK STAR, and $T_{trs} = 53.5^\circ\text{C}$ for

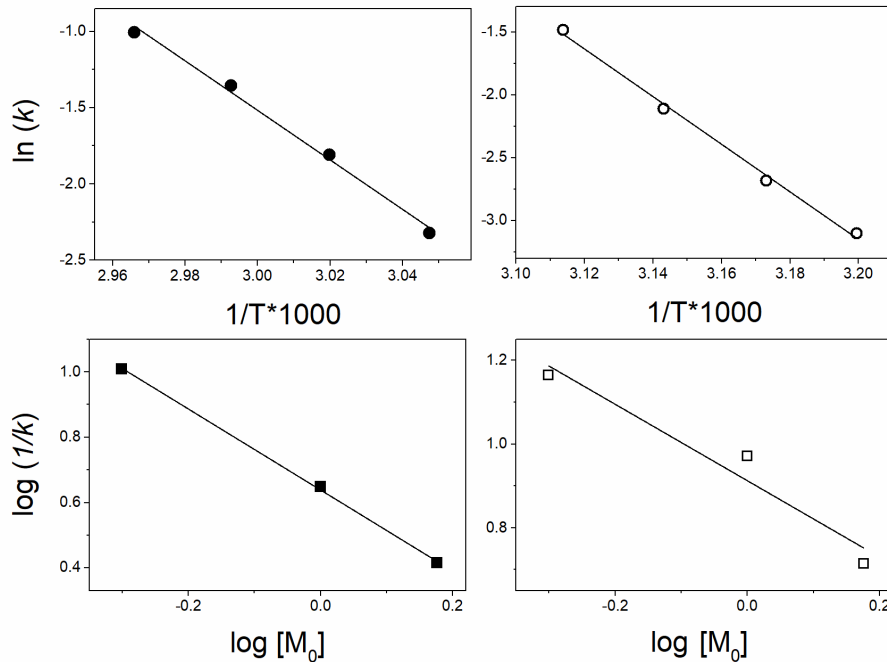


Figure 5. Dependences of rate constants of aggregation in dependence on temperature (upper row) and protein concentration (lower row) of two SAK variants: 42D (left column) and 42D 3A (right column). The linear dependences correspond to the functions described by Equations 3 and 4.

SAK STAR 3A (Figure S8). In the studied conditions the variants SAK STAR and SAK STAR 3A did not show signs of aggregation at T_{trs} and $T_{trs} + 3^{\circ}\text{C}$. Slight aggregation (10-20%) has been observed at $T_{trs}+6^{\circ}\text{C}$ and $T_{trs}+9^{\circ}\text{C}$. Therefore, we conclude that these variants can be considered as colloiddally stable.

On the other hand, the variants SAK 42D and SAK 42D 3A were significantly more pronounced to the aggregation. From the soluble protein decay kinetics, determined by an exponential decrease in absorbance (Equation 3), we have obtained activation energies of aggregation from Arrhenius equation (Equation 2) for SAK 42D and SAK 42D 3A, yielding ~ 135 kJ/mol and ~ 157 kJ/mol, respectively.

To obtain more detailed information regarding molecularity of the reaction, we analyzed colloidal stability of SAK 42D and SAK 42D 3A at $T_{trs}+3^{\circ}\text{C}$ at three different protein concentrations: 0.5, 1.0, and 1.5 mg/mL. The plots of $\log(I/k)$ vs $\log[M_0]$ for both SAK 42D variants show the linear dependences (Figure 5). From the Equation 4 we can calculate values n , reflecting the molecularity of the reactions. The obtained n values 2.2 and 1.9 for SAK 42D and SAK 42D 3A, respectively, clearly point out on an apparent second-order kinetics, which likely represent a limiting step in the intermolecular interaction followed by the aggregation.

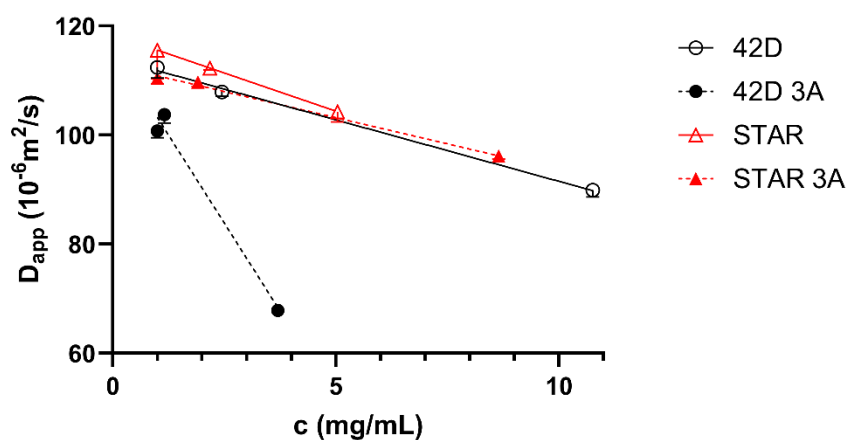


Figure 6. Linear fits of concentration dependency of apparent diffusion coefficient D_{app} for studied SAK variants as derived from DLS. Data points represent average with standard deviation from 10 measurements.

Dynamic and static light scattering of SAK variants. To further compare colloidal stability between SAK variants, we analysed concentration dependence of the apparent diffusion coefficient (D_{app}) at 25°C measured by DLS for SAK protein variants (Figure 6). In difference to aggregation rate determination at temperatures near to the temperature transition point for low protein concentration showed in the previous paragraph, correlation of D_{app} at a low temperature with changes in protein concentration reflects the repulsive or attractive protein

interactions [Bauer et al. 2016]. To increase the robustness of analysis we used three concentrations of proteins spanning approximately one order of magnitude. All proteins except SAK 42D 3A exhibited a linear dependence of D_{app} with a small negative slope, indicating weak attractive intermolecular forces, resulting in dimerization to various extents proportional to concentration (Table 1). In contrast, SAK 42D 3A exhibited much bigger negative slope, pointing to a strong attraction of molecules and increased tendency to aggregation. Indeed, this variant was stable at 3.7 mg/mL only up to 3 minutes and later started to gradually oligomerise, forming precipitated aggregates after 40 min (not shown). Similar distinction among samples was observed in polydispersity index. Apart from SAK 42D 3A, measured properties correspond to mono-modal and monodisperse solutions; estimated fraction of dimers was 16 - 100 % (Table 1). SAK 42D 3A variant exhibited a pronounced polydispersity in both medium and high concentrations (Table 1, Figure S9). As mentioned above, the high-concentration sample (3.7 mg/mL) was unstable at the measurement temperature (25°C), with gradually increasing R_h during the first 8 minutes of measurement, and completely aggregated later.

We further collected light-scattering data during the thermal scan, providing additional information on the changes in the molecular size and weight of SAK proteins in the region of thermal transition, thereby complementing the thermodynamic data obtained by DSC. Firstly, we determined a temperature transition point for thermally induced precipitation as monitored by an onset of decrease in protein solution transmittance as ~52 °C, 41 °C, 66 °C and 54 °C for SAK 42D, SAK 42D 3A, SAK STAR and SAK STAR 3A, respectively. The order of these aggregation temperatures corresponds well with the thermal transition temperatures of the studied SAK variants by DSC.

Table 1. Parameters obtained from DLS experiments conducted at medium and high protein concentration. nd – not determined due to aggregation								
SAK variant	Protein concentration (mg/mL)		Polydispersity (%)		Monomer (%)		Dimer (%)	
Protein/ concentration	Medium	High	Medium	High	Medium	High	Medium	High
SAK 42D	2.5	10.8	11.2	7.9	76	0	24	100
SAK 42D 3A	1.2	3.7	20.4	28.8	66	nd	34	nd
SAK STAR	2.2	5.0	5.8	9.2	84	66	16	34
SAK STAR 3A	1.9	8.7	8.3	3.1	79	30	21	70

Secondly, we adopted a combination of DLS and SLS data to dissect molecular unfolding and oligomerization of SAK variants at temperatures below the precipitation

transition point, which required the high sensitivity of DynaPro instrument. Autocorrelation functions of SAK variants fell into two major groups, with fast and slow correlation times corresponding to small and very big particles, before and after precipitation transition point, respectively. In addition to this, SAK STAR exhibited a third class of curves with multimodal character in the region 60-66 °C right before the transition point (Figure S10). Monomodal autocorrelation curves before the transition point can be evaluated by cumulants analysis. We analysed the temperature dependence of the R_h for SAK variants as derived from D_{app} using Stokes–Einstein–Sutherland equation, together with corresponding SLS intensities I_{SLS} (Figure 7). The combination of R_h and I_{SLS} allowed us to distinguish between an initial unfolding phase (increasing R_h under constant I_{SLS} , regions labelled U in Figure 7) and oligomerization phase (increasing both R_h and I_{SLS} , regions labelled O in Figure 7). SAK variants STAR, STAR 3A and 42D 3A exhibited at least partial monomer unfolding at the beginning of thermal transition, in the temperature window spanning 3-4 °C, whereas the SAK 42D passed nearly instantaneously from folded monomers to precipitates with only 1 °C narrow region of oligomeric transition. After the unfolding phase, 3A variants underwent monomodal oligomerization in the temperature window 3-4 °C with gradually increasing R_h to 5.5-7 nm, followed by precipitation transition point. In contrast, SAK STAR formed no monomodal oligomers but passed to the multimodal phase with coexisting (unfolded) monomers and large soluble oligomers (region labelled MO in Figure 7). It is important to consider that during thermal unfolding and/or oligomerization the assumption of molecule sphericity is likely violated, therefore the analysis by Stokes–Einstein–Sutherland equation reveals mostly trends of R_h change; however, in combination with I_{SLS} , one can distinguish the phase of monomer unfolding from the phase of oligomerization. Under the condition $R_h < 10 \text{ nm} \ll 658 \text{ nm}$ (the wavelength of scattered light), I_{SLS} itself is independent of molecular shape and the molecular form factor is equal to the unity, therefore, the I_{SLS} is directly proportional to the mass-averaged molecular weight of the protein particles [Wyatt 1993].

Summarizing, light scattering measurements revealed more molecular details about the conformational changes of SAK variants before the precipitation temperature transition point. It remains to be shown if these steps including unfolding and oligomerization are at least partially reversible.

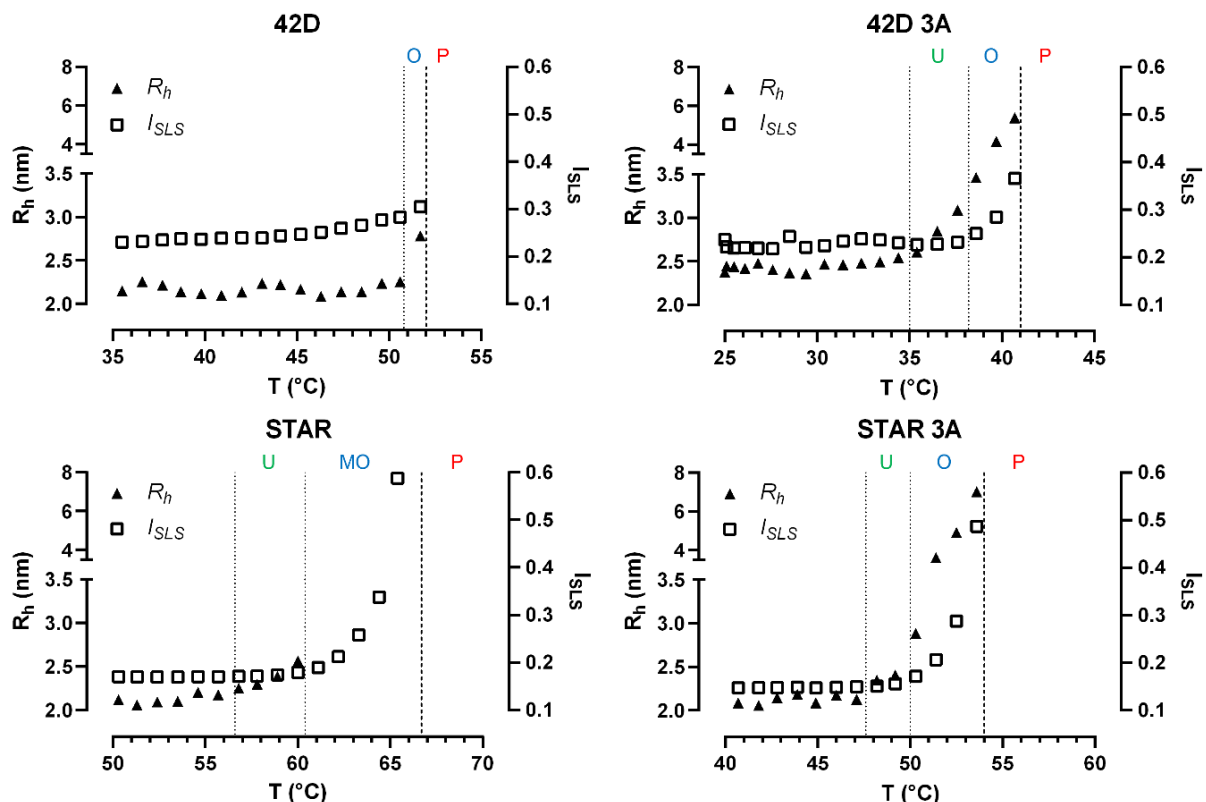


Figure 7. Analysis of hydrodynamic radius (R_h) and molecular weight of SAK variants in the thermal scan region preceding precipitation temperatures. Thermal unfolding is characterised by R_h increase in the range of ~2.1 nm (globular monomer) to ~3.4 nm (unfolded monomer) under constant SLS intensities (I_{SLS}), whereas during (monomodal) oligomerization, R_h rises simultaneously with I_{SLS} . Multimodal oligomerization of STAR variant implies simultaneous existence of monomeric and oligomeric species, in this condition no R_h from the cumulants analysis can be inferred. The dashed vertical lines indicate regions corresponding to distinct structural states observed during thermal scan: U – unfolding, O – (monomodal) oligomerization, MO – multimodal oligomerization, and P – precipitation.

Discussion

Detailed analysis of thermal denaturation of proteins is essential for proper determination of protein conformational and colloidal stabilities. This is particularly critical for therapeutic proteins, of which stability is a decisive property for their practical utilization. In fact, while low conformational stability of protein may compromise its shelf-life and function at physiological conditions, low colloidal stability may trigger undesirable immunological response [Lundahl et al. 2021].

Analysis of thermal denaturation of four variants of SAK, promising thrombolytics of the third generation [Nedaeinia et al. 2020], leads to several observations:

(i) Thermal denaturation of the SAK variants is scan rate- and protein concentration-dependent and is described by two consecutive irreversible steps. In the case of SAK 42D

variants, the first transition is endothermic (shows positive calorimetric enthalpy) (SAK 42D) or slightly exothermic (negative calorimetric enthalpy) (SAK 42D 3A), while in the case of STAR variants, the first step is always significantly exothermic. In all studied SAK variants, the second transition is endothermic.

(ii) From the heating scan rate dependences follow that mutations in STAR variants influence the E_a values of the individual step in such a way that they become less dependent on the scan rate when compared with SAK 42D variants. This suggests that in the SAK 42D variants, the first step is accompanied by a time-dependent conformational change that affects the activation energy of the second transition. However, in all studied SAK variants, the conformational change connected with the first step entropically stabilizes the second step, evidenced by an increase in T_2^* values of the second transition with the decreasing scan rate of heating.

One can speculate whether the protein conformational change triggered by the first transition is related to a conformational relaxation observed in SAK upon formation the complex with plasmin [Toul et al. 2022].

(iii) Protein concentration dependences reveal that E_{a2} of the second step decreases with increasing concentration in all SAK variants. At the same time, the T_2^* values increase by $\sim 30^\circ\text{C}$ and $\sim 20^\circ\text{C}$ for STAR and STAR 3A, respectively. The observed change in $T_2^* \sim 6^\circ\text{C}$ and $\sim -4^\circ\text{C}$ is significantly smaller for SAK 42D and SAK 42D 3A, respectively. This observation agrees with an increased tendency of aggregation of 42D variants, likely due to fast formation of the thermally-unfolded aggregation prone state of the 42D variants. On the other hand, the first transition is accompanied by small decrease in T_1^* in all variants and steep increase ($\sim 150\text{--}350\text{ kJ/mol}$) in E_{a1} values of STAR and 42D variants with protein concentration increased from 0.5 to 2.0 mg/mL. In these two variants, there is also apparent a narrowing of their DSC transitions in protein concentration dependent manner, suggesting oligomerization of the proteins. This observation goes along with experiments related to colloidal stability of all SAK variants suggesting dimerization. The increased E_{a1} values indicate that the dimerization occurs before the first transition.

However, a question arises why, despite similar tendencies in E_{a1} and T_1^* parameters, is the first transition endothermic in the SAK 42D variant and significantly exothermic in the SAK STAR variant. The answer likely originates in the introduced mutations in the SAK STAR variant, which might affect both dimerization and aggregation. Apparently, introducing two more positive charges in SAK STAR variants, H43R and G36R, did not significantly affect SAK dimerization as follows from DLS experiments and the mutations not only stabilize a SAK

conformation but also prevent protein aggregation. The aggregation-suppressing effect of these mutations may be the outcome of their stabilization impact, preventing thus the formation of aggregation-prone conformations [Seshadri et al. 2009], and/or of adding two positive charges with a potential effect on augmented protein solubility [Shaw et al. 2001, Trevino et al. 2007].

In the case of 42D, increasing temperature triggers a conformational change, which leads to dimerization due to a temperature-induced strengthening of hydrophobic interaction [Baldwin 1986]. Replacing three charged residues, K74A, R77A, and E75A, by hydrophobic alanine residues in the SAK 42D 3A variant may explain: (a) its increased tendency of aggregation by alleviating the rate-limiting step of dimer formation and thus (b) the loss of endothermic nature of the first transition. In fact, observation of negative enthalpy in DSC agrees with DSC analysis of irreversible protein thermal unfolding performed by Milardi and colleagues [Milardi et al. 1994]. In this study, the negative enthalpy has been shown to occur in the case of the decreased heat capacity change in the process of thermal denaturation. This

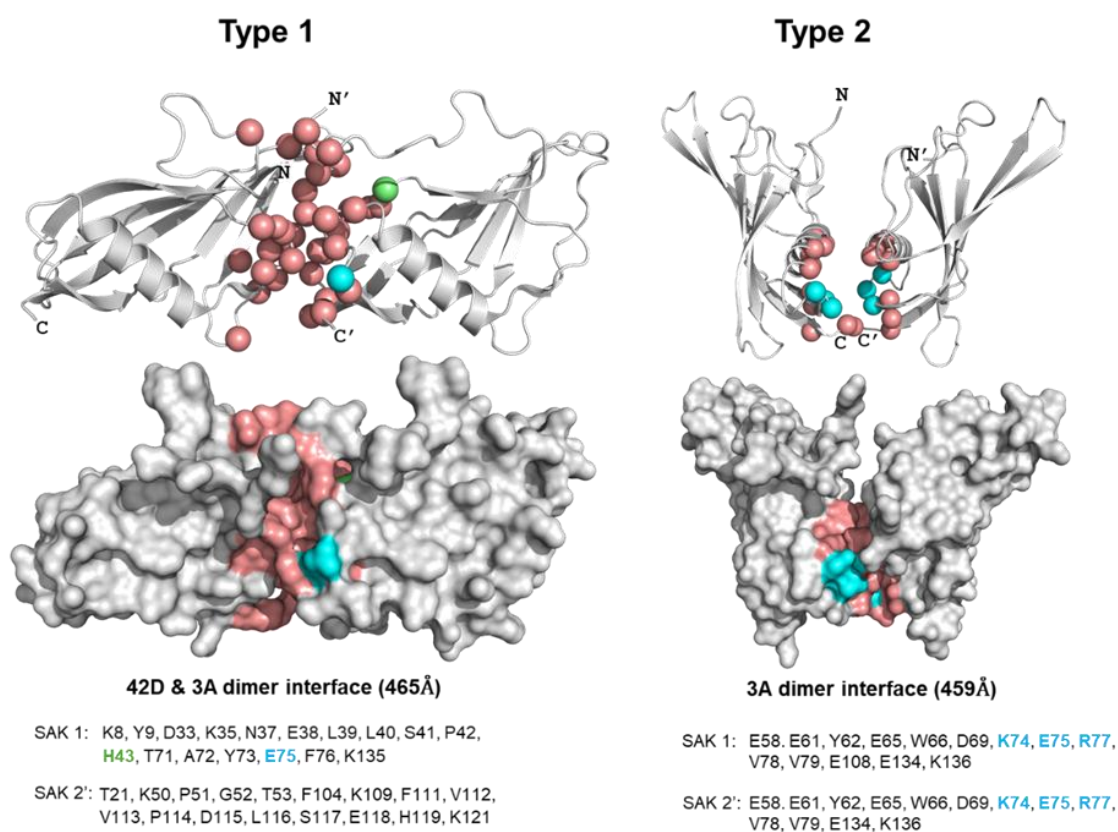


Figure 8. Structural models of two SAK dimer types (Type 1: PDB ID 1c77; Type 2: PDB ID 1c78) based on crystal structures reported by Chen et al. (2002). Top: ribbon representation with interface residues as spheres. Bottom: surface view of dimer interfaces. Type 1 dimer involves regions around residues S34, G36, and H43 (pink/green) and residues K74, E75, R77 (cyan), with only H43 and E75 directly contributing to the intermolecular contact. In contrast, the Type 2 dimer interface includes residues K74, E75, and R77 coming from both monomer units, and all of them interact directly across the interface; the region around S34, G36, and H43 is not involved.

assumes a decrease of hydrophobic surface [Myers et al. 1995], which is in the case of SAK variants a consequence of intermolecular interaction due to protein dimerization.

Detailed analysis of crystal structures of SAK presented in the work of Chen et al. [Chen et al. 2002] provides an alternative explanation of the observed differences in DSC behavior of studied SAK variants. Based on this crystallization study, SAK forms two distinct dimers denoted Type 1 dimer and Type 2 dimer, which are relevant for our analysis (Figure 8).

In Type1 dimer, the intermolecular interface of size 465 \AA^2 encompasses both positions K74, E75, and R77 mutated in SAK 3A, as well as positions S34, G36, and H43 mutated in SAK STAR. Of these six positions, only H43 and E75 are involved in direct intermolecular interaction with the SAK dimer counterpart. On the other hand, in the Type 2 dimer, of similar size of intermolecular dimerization interface, all three 3A residues (K74, E75, and R77) are involved in direct interdimeric interaction.

Based on these observations, we can speculate that Type 1 dimer is formed particularly by stable and thus likely rigid STAR variants. Our analysis of colloidal stability of SAK 42D variant strongly indicates dimer formation. However, it is unlikely that SAK 42D variant forms Type 2 dimer due to the presence of charged residues K74, E75, and R77 at the dimer interface in close proximity. Therefore, SAK 42D likely forms Type 1 dimer, but due to buried charged residues, the dimer may adopt a suboptimal conformation. It is possible that increased temperature-induced conformational change (demonstrated by positive enthalpy of the first transition) then leads to dimer formation. On the other hand, replacement of charged residues in SAK 42D 3A for alanine will likely result in Type 2 dimer formation.

The above analysis in regards colloidal stabilities of the studied SAK variants is summarized in Figure 9.

Importantly, dimerization and early-stage aggregation may also occur before therapeutic application - during storage, transport, or formulation of the protein. Such pre-formed dimers can reduce bioactivity and, in some cases, enhance immunogenicity upon administration. In fact, in our very recent work [Štulajterová et al. 2025], we showed that the SAK STAR variants exhibit higher activity than the SAK 42D variants. This behavior reflects an increased tendency of the 42D variants to form dimers and higher-order species, which are expected to represent catalytically less active forms due to reduced accessibility of functional binding interfaces. To suppress unwanted dimerization, formulation additives that stabilize the monomeric state can be employed [Mao et al. 2025]. Arginine, for example, has been shown to suppress both reversible and irreversible aggregation by screening surface charges and minimizing hydrophobic interactions, thereby stabilizing native conformations [Schaefer et al.

2018, Arakawa et al. 2007]. Implementing such charge-stabilizing excipients could significantly improve formulation robustness of SAK-based thrombolytic agents.

From a translational perspective, clinically used non-immunogenic staphylokinase (Fortelyzin®) is administered as a single intravenous bolus of 15 mg reconstituted in 15 mL of saline, corresponding to an approximate protein concentration of ~1 mg/mL at administration [Leontyev et al. 2025]. The concentrations investigated here (0.5-2.0 mg/mL in DSC and up to ~10 mg/mL in selected light-scattering experiments) therefore encompass and moderately exceed the clinically relevant range. Higher concentrations were intentionally employed as part of an accelerated stability approach to amplify intermolecular interactions and reveal latent tendencies toward dimerization and aggregation. This strategy enabled detection of concentration-dependent association processes that may become relevant during manufacturing, storage, reconstitution, or temperature excursions, thereby strengthening the predictive value of the biophysical analysis for practical applications.

The present results provide direct guidance for rational engineering and formulation of future SAK variants. Our data demonstrate that relatively small changes in surface charge distribution strongly modulate dimerization mode, aggregation propensity, and kinetic stability. Variants with more favorable electrostatic surface patterns (STAR background) preferentially

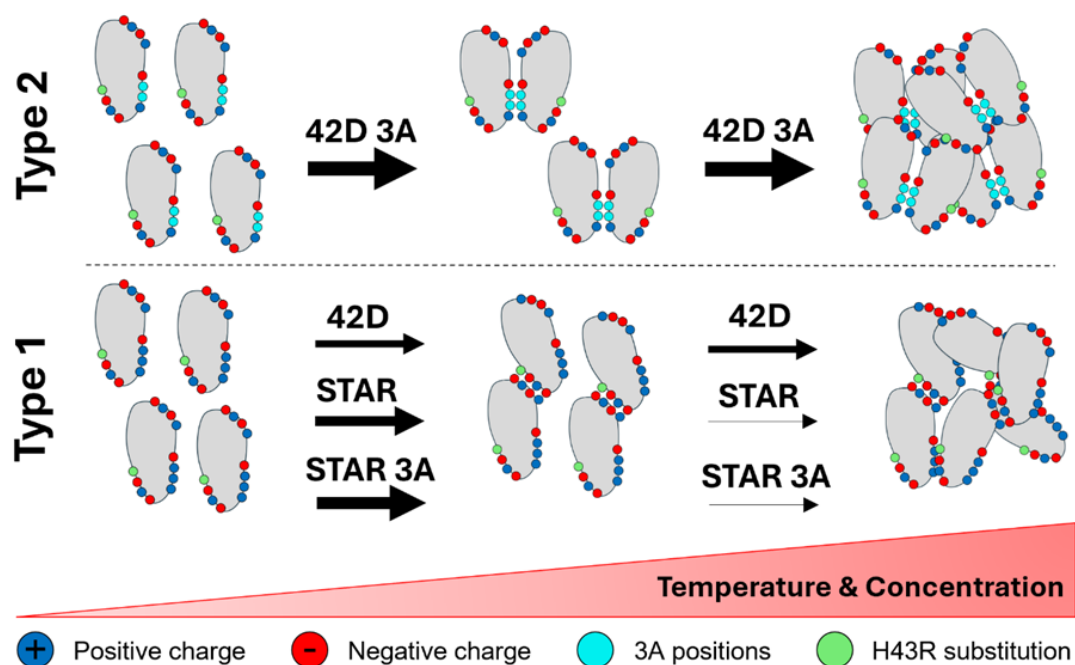


Figure 9. Schematic illustration of two proposed dimerization modes for SAK variants based on model-derived interpretation under increasing temperature and protein concentration. Most SAK variants predominantly form Type 1 dimers stabilized by charge complementarity, whereas SAK 42D 3A preferentially forms a Type 2 dimer driven by hydrophobic interactions involving the 3A substitutions.

form weakly associating, aggregation-resistant dimers, whereas increased hydrophobic exposure at dimer interfaces (42D and especially 42D 3A) promotes rapid irreversible aggregation. This indicates that future sequence engineering should prioritize tuning surface charge balance at interface regions (residues 34-36-43 and 74-77) to suppress hydrophobically driven intermolecular contacts while preserving catalytic function and low immunogenicity. Because thermal denaturation is kinetically controlled, activation energies and T parameters derived from DSC represent sensitive screening metrics for identifying aggregation-prone variants early in development. In parallel, formulation strategies based on charge-screening and aggregation-suppressing excipients, as well as optimized protein concentration, may further stabilize the monomeric or weakly associated states and improve long-term robustness of SAK-based therapeutics.

In conclusion, our results show that SAK undergoes temperature- and concentration-dependent dimerization in aqueous solution. The SAK variants investigated in this study differ substantially in their dimerization behavior, conformational and colloidal stabilities, and consequently in their functional properties, owing to differences in their primary sequences. Through comparative biophysical analyses, we were able to rationalize these differences in terms of engineered surface charge distributions, which govern both dimerization and aggregation propensities. These insights are not only essential for guiding the rational design of future SAK mutants with improved stability and reduced immunogenicity but are also highly relevant for optimizing formulation strategies-including excipient selection and storage conditions - for the development of clinically viable thrombolytic agents.

Acknowledgements

This work has been funded by the EU NextGenerationEU through the Recovery and Resilience Plan for Slovakia under the projects 09I01-03-V04-00041, 09I03-03-V04-00116 and No. 09-I02-03-V01-00021. This project was also supported by the European Union's Horizon 2020 Research and Innovation Programme under the grant agreements CETOCOEN (No. 857560) and CLARA (No. 101136607). Authors thank the RECETOX Research Infrastructure (No. LM2023069) and CZECRIN (LM2023049) financed by the Ministry of Education, Youth and Sports for supportive background.

References

- Alasheev AM, Lantsova EV, Tretyakov DA (2023) [Efficacy and safety of non-immunogenic staphylokinase in the ischemic stroke in real-world clinical practice in the Sverdlovsk region]. *Zhurnal Nevrologii I Psikiatrii Imeni S.S. Korsakova* 123(7): 74–79. <https://doi.org/10.17116/jnevro202312307174>.
- Arakawa T, Ejima D, Tsumoto K, Obeyama N, Tanaka Y, Kita Y, Timasheff SN (2007) Suppression of protein interactions by arginine: A proposed mechanism of the arginine effects. *Biophysical Chemistry* 127(1-2): 1-8. doi: 10.1016/j.bpc.2006.12.007.
- Baldwin RL (1986) Temperature dependence of the hydrophobic interaction in protein folding. *Proc. Natl. Acad. Sci. U.S.A.* 83(21): 8069-8072. doi: 10.1073/pnas.83.21.8069.
- Bauer KC, Göbel M, Schwab ML, Schermeyer MT, Hubbuch J (2016) Concentration-dependent changes in apparent diffusion coefficients as indicator for colloidal stability of protein solutions. *Int. J. Pharm.* 511(1): 276-287. doi: 10.1016/j.ijpharm.2016.07.007.
- Behnke D, Gerlach D (1987) Cloning and expression in *Escherichia coli*, *Bacillus subtilis*, and *Streptococcus sanguis* of a gene for staphylokinase - a bacterial plasminogen activator. *Mol. Gen. Genet.* 210(3): 528-534. doi: 10.1007/BF00327208.
- Brandts JF, Lin LN. Study of strong to ultratight protein interactions using differential scanning calorimetry. *Biochemistry*. 1990 Jul 24;29(29):6927-40. doi: 10.1021/bi00481a024.
- Carrillo RJ, Semple A (2024) DSC Derived (E_a & ΔG) Energetics and Aggregation Predictions for mAbs. *J. Pharm. Sci.* 113(8): 2140-2150. doi: 10.1016/j.xphs.2024.05.009
- Chen Y, Mao H, Zhang X, Gong Y, Zhao N (1999) Thermal conformational changes of bovine fibrinogen by differential scanning calorimetry and circular dichroism. *Int. J. Biol. Macromol.* 26(2-3): 129-134. doi: 10.1016/s0141-8130(99)00073-2.
- Chen Y, Song G, Jiang F, Feng L, Zhang X, Ding Y, Bartlam M, Yang A, Ma X, Ye S, Liu Y, Tang H, Song H, Rao Z (2002) Crystal structure of a staphylokinase: variant a model for reduced antigenicity. *Eur. J. Biochem.* 269(2): 705-711. doi: 10.1046/j.0014-2956.2001.02706.x.
- Collen D, Silence K, Demarsin E, De Mol M, Lijnen HR (1992) Isolation and characterisation of natural and recombinant staphylokinase. *Fibrinolysis* 6(4): 203-213. doi:10.1016/0268-9499(92)90073-Q.
- Collen D (1997) Thrombolytic therapy. *Thromb. Haemost.* 78(1): 742-746. PMID: 9198249.

- Collen D, Stockx L, Lacroix H, Suy R, Vanderschueren S (1997) Recombinant staphylokinase variants with altered immunoreactivity. IV: Identification of variants with reduced antibody induction but intact potency. *Circulation* 95(2): 463-472. doi: 10.1161/01.cir.95.2.463.
- Frokjaer S, Otzen DE (2005) Protein drug stability: a formulation challenge. *Nat. Rev. Drug Discov.* 4(4): 298-306. doi: 10.1038/nrd1695.
- Gusev EI, Martynov MY, Nikonov AA, Shamalov NA, Semenov MP, Gerasimets EA, Yarovaya EB, Semenov AM, Archakov AI, Markin SS, FRIDA Study Group. (2021). Non-immunogenic recombinant staphylokinase versus alteplase for patients with acute ischaemic stroke 4-5 h after symptom onset in Russia (FRIDA): A randomised, open label, multicentre, parallel-group, non-inferiority trial. *The Lancet. Neurology* 20(9): 721–728. [https://doi.org/10.1016/S1474-4422\(21\)00210-6](https://doi.org/10.1016/S1474-4422(21)00210-6)
- Gütthe S, Kapinos L, Möglich A, Meier S, Grzesiek S, Kiefhaber T (2004) Very fast folding and association of a trimerization domain from bacteriophage T4 fibrin. *J. Mol. Biol.* 337(4): 905-915. doi: 10.1016/j.jmb.2004.02.020.
- Koppel DE (1972) Analysis of Macromolecular Polydispersity in Intensity Correlation Spectroscopy: The Method of Cumulants. *J. Chem. Phys.* 57, 4814–4820.
- Lack CH (1948) Staphylokinase; an activator of plasma protease. *Nature* 161 (4093): 559. <https://doi.org/10.1038/161559b0>.
- Leontyev SG, Yarovaya EB, Kutsenko VA, Ivlev OE, Soplenskova AG, Semenov AM, Semenov MP, Ivanov SV, Romashova YA, Markin SS (2025) The Safety of Non-immunogenic Recombinant Staphylokinase in Elderly Patients With Massive Pulmonary Embolism: A Randomized Clinical Trial FORPE. *Health Sci. Rep.* 8(5): e70826. doi: 10.1002/hsr2.70826.
- Lijnen HR, Van Hoef B, De Cock F, Okada K, Ueshima S, Matsuo O, Collen D (1991) On the mechanism of fibrin-specific plasminogen activation by staphylokinase. *J. Biol. Chem.* 266 (18): 11826-11832.
- Lundahl MLE, Fogli S, Colavita PE, Scanlan EM (2021) Aggregation of protein therapeutics enhances their immunogenicity: causes and mitigation strategies. *RSC Chem. Biol.* 2: 1004-1020. doi: 10.1039/d1cb00067e.
- Lyubarev AE, Kurganov BI (1998) Modeling of irreversible thermal protein denaturation at varying temperature. I. The model involving two consecutive irreversible steps. *Biochemistry (Mosc).* 63(4): 434-440. PMID: 9556526.

- Mao T, Xu X, Winkler PM, Siri C, Poliukhina E, Silva PJ, Xu N, Hu Y, Zahabi KA, Polla RL, Luo Z, Ong Q, Alexander-Katz A, Stellacci F (2025) Stabilizing effect of amino acids on protein and colloidal dispersions. *Nature* 645: 915–921. doi: 10.1038/s41586-025-09506-w.
- Milardi D, La Rosa C, Grasso D (1994) Extended theoretical analysis of irreversible protein thermal unfolding. *Biophys. Chem.* 52(3): 183-189. doi: 10.1016/0301-4622(94)00033-g.
- Myers JK, Pace CN, Scholtz JM (1995) Denaturant m values and heat capacity changes: relation to changes in accessible surface areas of protein unfolding. *Protein Sci.* 4(10): 2138-2148. doi: 10.1002/pro.5560041020.
- Nedaeinia R, Faraji H, Javanmard SH, Ferns GA, Ghayour-Mobarhan M, Goli M, Mashkani B, Nedaeinia M, Haghighi MHH, Ranjbar M (2020). Bacterial staphylokinase as a promising third-generation drug in the treatment for vascular occlusion. *Mol. Biol. Rep.* 47(1): 819-841. <https://doi.org/10.1007/s11033-019-05167-x>.
- Nemergut M, Škrabana R, Berta M, Plückthun A, Sedlák E (2021) Purification of MBP fusion proteins using engineered DARPIn affinity matrix. *Int. J. Biol. Macromol.* 187: 105-112. doi: 10.1016/j.ijbiomac.2021.07.117.
- Nemergut M, Sedláková D, Fabriciová G, Belej D, Jancura D, Sedlák E (2023) Explanation of inconsistencies in the determination of human serum albumin thermal stability. *Int. J. Biol. Macromol.* 232: 123379. doi: 10.1016/j.ijbiomac.2023.123379.
- Nikitin D, Choi S, Mican J, Toul M, Ryu W-S, Damborsky J, Mikulik R, Kim D-E (2021). Development and testing of thrombolytics in stroke. *J. Stroke* 23(1): 12-36. <https://doi.org/10.5853/jos.2020.03349>
- Pina DG, Gómez J, Villar E, Johannes L, Shnyrov VL (2003) Thermodynamic analysis of the structural stability of the shiga toxin B-subunit. *Biochemistry* 42(31): 9498-9506. doi: 10.1021/bi034591s.
- Provencher SW (1979) Inverse Problems in Polymer Characterization: Direct Analysis of Polydispersity with Photon Correlation Spectroscopy. *Die Makromolekulare Chemie* 180, 1: 201–209.
- Ramsay G, Montgomery D, Berger D, Freire E (1989) Energetics of diphtheria toxin membrane insertion and translocation: calorimetric characterization of the acid pH induced transition. *Biochemistry* 28(2): 529-533. doi: 10.1021/bi00428a018.
- Ramsay G, Freire E (1990) Linked thermal and solute perturbation analysis of cooperative domain interactions in proteins. Structural stability of diphtheria toxin. *Biochemistry* 29(37): 8677-8683. doi: 10.1021/bi00489a024.

- Ratanji KD, Derrick JP, Dearman RJ, Kimber I (2013) Immunogenicity of therapeutic proteins: Influence of aggregation. *J Immunotoxicol.* 11(2):99–109. doi: 10.3109/1547691X.2013.821564.
- Sánchez-Ruiz JM, López-Lacomba JL, Cortijo M, Mateo PL (1988) Differential scanning calorimetry of the irreversible thermal denaturation of thermolysin. *Biochemistry* 27(5): 1648-1652. doi: 10.1021/bi00405a039.
- Sanchez-Ruiz JM (1992) Theoretical analysis of Lumry-Eyring models in differential scanning calorimetry. *Biophys. J.* 61 (4): 921-935. doi: 10.1016/S0006-3495(92)81899-4.
- Schaefer JV, Sedlák E, Kast F, Nemergut M, Plückthun A (2018) Modification of the kinetic stability of immunoglobulin G by solvent additives. *Mabs.* 10(4):607-623. doi: 10.1080/19420862.2018.1450126.
- Sedlák E, Schaefer JV, Marek J, Gimeson P, Plückthun A (2015) Advanced analyses of kinetic stabilities of iggs modified by mutations and glycosylation. *Protein Sci.* 24(7): 1100-1113. doi: 10.1002/pro.2691.
- Seshadri S, Oberg KA, Uversky VN (2009) Mechanisms and consequences of protein aggregation: the role of folding intermediates. *Curr. Protein Pept. Sci.* 10(5): 456-463. doi: 10.2174/138920309789351976.
- Shaw KL, Grimsley GR, Yakovlev GI, Makarov AA, Pace CN (2001) The effect of net charge on the solubility, activity, and stability of ribonuclease Sa. *Protein Sci.* 10(6): 1206-1215. doi: 10.1110/ps.440101.
- Sturtevant JM (1987) Biochemical applications of differential scanning calorimetry. *Annu. Rev. Phys. Chem.* 38: 463-488. doi: 10.1146/annurev.pc.38.100187.002335.
- Štulajterová M, Ambro L, Sedláková D, Nemergut M, Kohout P, Mazurenko S, Varhač R, Strunga A, Toul M, Prokop Z, Damborský J, Tomková M, Sedlák E (2025) Assessing the impact of His-tags on activity and stability of staphylokinase variants. *Int. J. Biol. Macromol.* 328(Pt 2): 147655. doi: 10.1016/j.ijbiomac.2025.147655.
- Toul M, Nikitin D, Marek M, Damborsky J, Prokop Z (2022) Extended Mechanism of the Plasminogen Activator Staphylokinase Revealed by Global Kinetic Analysis: 1000-fold Higher Catalytic Activity than That of Clinically Used Alteplase. *ACS Catal.* 12 (7), 3807-3814. doi: 10.1021/acscatal.1c05042.
- Trevino SR, Scholtz JM, Pace CN (2007) Amino acid contribution to protein solubility: Asp, Glu, and Ser contribute more favorably than the other hydrophilic amino acids in RNase Sa. *J. Mol. Biol.* 366(2): 449-460. doi: 10.1016/j.jmb.2006.10.026.

- Vanderschueren SM, Stassen JM, Collen D (1994). On the immunogenicity of recombinant staphylokinase in patients and in animal models. *Thrombosis and Haemostasis* 72 (2): 297–301.
- Wyatt PJ (1993) Light Scattering and the Absolute Characterization of Macromolecules. *Anal. Chim. Acta* 272, 1: 1–40.